PAPER

Check for updates

Toughened chitosan-based composite membranes with antibiofouling and antibacterial properties via incorporation of benzalkonium chloride†

Fitri Khoerunnisa, [ID] [a] Chintia Kulsum,[a] Fitri Dara,[b] Mita Nurhayati, [ID] [a] Nisa Nashrah,[c] Siti Fatimah,[c] Amelinda Pratiwi,[a] Hendrawan Hendrawan,[a] Muhamad Nasir, [ID] [b] Young Gun Ko, [ID] [c] Eng-Poh Ng [ID] [d] and Pakorn Opaprakasit [ID] *[e]

Biofouling due to biofilm formation is a major problem in ultrafiltration membrane applications. In this work, a potential approach to solve this issue has been developed by functionalization of chitosan-based membranes with benzalkonium chloride (BKC). The chitosan composite membranes consisting of poly(ethylene glycol) (PEG), multiwalled carbon nanotubes (MWCNT), and BKC were synthesized by mixing the membrane precursors and the antibacterial solution, and casting via an inversed phase technique. The effects of the BKC content on the morphology and performance of the membranes are investigated by varying the BKC feed compositions. The composite membranes demonstrate better antibacterial efficacy against *Staphylococcus aureus* than *Escherichia coli*. The permeability and selectivity performances of the composites as filter membranes are examined by employing a dead-end filtration system. Interestingly, enhanced toughness of the membranes is observed as a function of the BKC content. Mechanisms of the structural formation are investigated. The results from SEM, XRD, and FTIR spectroscopy revealed that MWCNT/BKC are located as nanoclusters with $\pi-\pi$ stacking interactions, and are covered by PEG chains. The shape of the dispersed domains is spherical at low BKC contents, but becomes elongated at high BKC contents. These act as soft domains with an anisotropic shape with toughening of the brittle chitosan matrix, leading to enhanced durability of the membranes, especially in ultrafiltration applications. The composite membranes also demonstrate improved rejection in dead-end ultrafiltration systems due to high porosity, high hydrophilicity, and the positive charges of the membrane surface.

1. Introduction

Chitosan is an abundantly-available biopolymer, which can be derived from crustacean shell wastes. Chitosan is a derivatized polysaccharide with attractive properties, due to its modifiability. The presence of hydroxyls and amines on its polymeric chains makes it easily chemically modified. It can also be manufactured in a variety of forms including sponge, fiber, gel,

[a]Department of Chemistry, Indonesia University of Education, Setiabudhi 229, Bandung 40154, Indonesia

[b]Research Unit for Clean Technology, Indonesian Institute of Science, Bandung 40135, Indonesia

[c]School of Material Science & Engineering, Yeungnam University, Gyeongsan 38541, South Korea

[d]School of Chemical Sciences, Universiti Sains Malaysia, 11800 USM, Penang, Malaysia

[e]School of Bio-Chemical Engineering and Technology, Sirindhorn International Institute of Technology (SIIT), Thammasat University, Pathum Thani 12121, Thailand. E-mail: pakorn@siit.tu.ac.th

† Electronic supplementary information (ESI) available. See DOI: 10.1039/d1ra01830b

and membrane.[1] A chitosan-based membrane is recognized as a potential bio-based/degradable membrane for separation technology.[2] However, several disadvantages, *i.e.*, low porosity, poor mechanical strength, and low hydrophilicity are still obstacles for practical use. Many fabrication approaches for the chitosan-based membranes with improved properties have been reported to overcome these limitations. These approaches include hydrophilic monomer grafting onto the membrane surface,[3,4] hydrophilic monomer interfacial polymerization,[5] polymer chain functionalization,[6] composite formation by incorporation of inorganic materials,[7–9] and embedding with nanoparticles.[10,11]

In recent decades, chitosan composite membranes have been commonly utilized in water and wastewater treatments.[12–14] Biofouling, however, is still the main issue affecting the efficiency of membrane filtration with a shortened membrane lifetime due to biofilm formation by bacteria.[15,16] Biofouling occurs because of bacterial adhesion to the membrane surface in a form of biofilms, leading to the agglomeration of soluble particulate matter on membrane surface and pores.[17] This process may adversely lead to a drop in

the permeate flux,[12] reducing the efficiency of the membrane. It is also beneficial to have antibiofouling-capable membranes.[18]

Since biofouling is an unavoidable phenomenon, different techniques have been introduced to inhibit bacteria from attaching to the membrane surface. Several approaches to biofouling management have been used. Various surface modifications have been shown to be appropriate methods in controlling the fouling of membranes, such as hydrophobic or hydrophilic and electropositive or electronegative modifications. Currently, incorporation of hybrid materials, such as metal,[8,19–21] metal oxide,[22,23] iodine,[24] sodium lignosulfonate,[25] cationic surfactant,[26] and quaternary ammonium compounds (QACs)[27–29] as antibacterial agents have been explored for antifouling properties.

QACs have been integrated into polymeric membranes in recent years to reduce biofouling based on contact-killing mechanisms.[27–30] It has been shown that QACs demonstrate effective antibacterial activity by introducing their long alkyl chains into the membrane of a bacterium. QACs also modify the phospholipid bilayer, disrupting the integrity of the membrane. This contributes to the leakages of cellular contents.[31] Among these, benzalkonium chloride (BKC) is one of the most widely used[32–34] because of its relatively low toxicity to humans, mild persistence in the environment, and high efficiency in killing bacteria[33] and fungi.[35] When added into bulk materials, BKC adds antimicrobial properties. This enables the development of facile approaches to develop antimicrobial bulk materials such as membranes.

Multi-walled carbon nanotubes (MWCNTs) are carbon materials consisting of multiple rolled layers or tubes of graphene. With their small sizes, high aspect ratio, high strength, and stiffness, MWCNTs have a high potential for use as reinforcing agents for various materials.[36] They are especially useful in polymeric biomaterials, to attain better biomechanical properties.[37] In preparing polymeric membranes with a macroporous structure, poly(ethylene glycol) (PEG) is commonly employed as a porogen. The addition of PEG has contributed to the formation of more porous polymeric materials and a higher swelling ratio.[38] In our previous work, chitosan/PEG/MWCNT membranes were fabricated for use in the treatment of dye wastewaters.[24] The membranes showed good antimicrobial properties with the incorporation of iodine. In spite of, a reduction in the membrane's strength was noticed with an addition in iodine concentration. This is likely due to its high reactivity to complex and react with chitosan structures,[39] which adversely affect the toughness of the membranes and their durability.

This study is aimed to prepare composite membranes based on the chitosan/PEG/MWCNT system with an antimicrobial and antibiofouling agent on their surfaces. BKC is chosen as the antimicrobial and antibiofouling agent. The effects of the BKC feed composition on the antibacterial properties of the membranes are examined against two bacteria, *Escherichia coli* (*E. coli*) and *Staphylococcus aureus* (*S. aureus*). To show the effects of BKC on the properties of composite membranes, morphology and function of the synthesized membranes are characterized. Interestingly, enhanced toughness of the membranes is observed as a function of the BKC content. The

mechanisms of the structural formation are therefore investigated. The performance of the composites as filter membranes, *i.e.*, permeability and selectivity, is examined by employing a dead-end filtration system.

2. Experimental

2.1. Materials

Chitosan ($M_w \sim 33\,000$ Da, DD = 87.5%), PEG ($M_n = 6000$ g mol^{-1}), benzalkonium chloride ($C_6H_5CH_2N(CH_3)_2RCl$, R = C_8H_{17}) acetic acid (CH_3COOH, 1%), sodium hydroxide (NaOH, 99%), Bovine Serum Albumin (BSA, $M_w \sim 66$ kDa), and azo blue dyes ($C_{34}H_{25}N_5Na_2O_{10}S_2$, $M_w = 7.74$ kDa) were obtained from Merck (Germany). Multi-walled carbon nanotubes (MWCNTs, average bundle size = 20 nm) were obtained from Wako Chemicals (Japan). Phosphate-buffered saline (PBS), plate count agar (PCA), Luria-Bertani (LB), *E. coli* strain (ATCC 25922), and *S. aureus* strain (ATCC 25923) were provided by Biofarma (Indonesia).

2.2. Methods

2.2.1. Synthesize of composite membranes. Chitosan-based composite membranes were synthesized by a phase inversion technique. A chitosan solution (3% w/v) was prepared by dissolving chitosan in acetic acid solution by continuous stirring at 500 rpm and 25 °C for 24 h. Solutions of PEG (2 wt%), BKC (1–12 wt%), and MWCNT dispersion (0.001 wt%) were also prepared in water. All prepared solutions were then mixed homogeneously for 10 min with magnetic stirring (volume ratio of chitosan : BKC : PEG : MWCNT of 8 : 2.5 : 4 : 3). The mixture was cast on a plate mould, followed by solvent evaporation. The resulting samples were immersed in NaOH solution (1.0 M) to discharge excess acetic acid and to release the membranes from the plate. The obtained membranes were then washed with deionized water and dried at 40 °C for a day. The M0 corresponds to chitosan/PEG/MWCNT composite and BKC loaded composite membrane at loading concentration of 60, 80, 100, and 120 ppm are named MB-60, MB-80, MB-100, and MB-120 respectively.

2.2.2. Membranes characterization. The interaction of functional groups in the membrane samples were characterized by Fourier transform infrared (FTIR) spectroscopy (Thermo Scientific Nicolet 6700 spectrometer) in ATR mode at 2 cm^{-1} resolution and 50 scans. The membrane crystallinity was determined by X-ray diffraction (Rigaku D-Max 2500; Cu Kα radiation, λ = 0.154 nm, 50 kV, 300 mA). The membrane morphology was examined using scanning electron microscopy (FE-SEM, Hitachi S-4800). The topographical profile of membranes was observed by atomic force microscopy (AFM, PARK XE-100). The thermal stability of the membrane was investigated by a thermogravimetric analyzer (Hitachi STA 7200).

The hydrophilicity of the composite membranes was determined using water contact angle (WCA) measurements. A droplet of water (4 µL) was applied onto a surface of a dried membrane using a micro-syringe. A picture was captured from the side view, and the WCA was determined using ImageJ software. Mechanical strength of the membranes was examined following the ASTM D882 standard using Shimadzu EZ-LX-500M.

To investigate the porosity of membrane (ε), a dry membrane was soaked in deionized water (25 °C, 24 h), and then dried with a filter paper before its weight was recorded. The membrane was further dried (50 °C, 24 h), and weighed. The membrane porosity was calculated using the equation reported in a previous work.[24] The average pore size (r_m) of the membranes was calculated using the Guerout–Elford–Fery equation.[40]

2.2.3. Antibacterial testing. The antibacterial activity of a chitosan-based membrane and BKC-loaded composite membranes toward a Gram-positive bacterium (*S. aureus*) and a Gram-negative bacterium (*E. coli*) was examined by disc diffusion (DD) and total plate counting (TPC) methods, under sterile conditions.[41] The DD method was selected to determine the minimum inhibitory concentration (MIC) of BKC in the membrane. UV-sterilized discs ($\varnothing$ 5 mm) were prepared from the membranes for DD assay. As a positive control, a disc of filter paper ($\varnothing$ 5 mm) was immersed in chloramphenicol (500 ppm). The negative control was immersed in sterile distilled water.[40–42] LB agar was poured onto the plate and allowed to solidify. The cultures of *E. coli* dan *S. aureus* were inoculated in LB broth (37 °C, 4–8 h), and then diluted in PBS solution to 1.5 $\times$ 10^8 cfu mL^{-1} (McFarland solution, 0.5 OD). 10 μL of bacteria suspension was then spread on the whole surface of the firm LB agar. All prepared discs were placed on the top of a treated LB agar plate. The prepared plates were incubated at 37 °C for 16–24 h. The zones of inhibition (ZOI) surrounding the filter disc due to the antibacterial activity of BKC-loaded membranes were observed and measured (in mm). A TPC method was used to determine the bacteria-killing ratio (BKR) of the BKC-loaded membranes, as previously described.[24]

2.2.4. Evaluation of membrane performance. The membrane performance on filtration was examined using a dead-end filtration model, as previously described.[24] The membrane permeability was calculated in terms of the permeation flux of deionized water. The rejection of membrane was evaluated by feeding azo blue dyes and a BSA solution (pH 7.3) at 2 bar.[24] The feed, permeate, and retentate concentrations of the dyes and BSA solutions were examined using a UV-Vis spectrophotometer (UV Mini Shimadzu-1240) at wavelengths of 595 and 280 nm for azo blue dyes and BSA solutions, respectively.

3. Results and discussion

3.1. Antibacterial efficacy

The antibacterial activity of the membranes was evaluated *via* the DD method. Fig. 1a shows the zone of inhibition (ZOI) of the prepared membranes, which begins to appear at MB-80 (ZOI = 7.5 mm) for *S. aureus* and MB-100 (ZOI = 8 mm) for *E. coli*. This reflects the minimum concentration of BKC required to inhibit bacteria growth. Interestingly, MB-120 demonstrated the largest ZOI for both bacteria, while an insignificant ZOI was observed in M-0. Additionally, BKC exhibits stronger inhibition activity towards *S. aureus* than that of *E. coli* (Fig. 1b), as indicated by the bacteria-killing ratio. M-0 has low antibacterial activity with a BKR of 16 and 2.6% for *E. coli* and *S. aureus*, respectively (Fig. 1c). This bacteriocidal ability is likely promoted by the antibacterial activity of the precursors of the composite
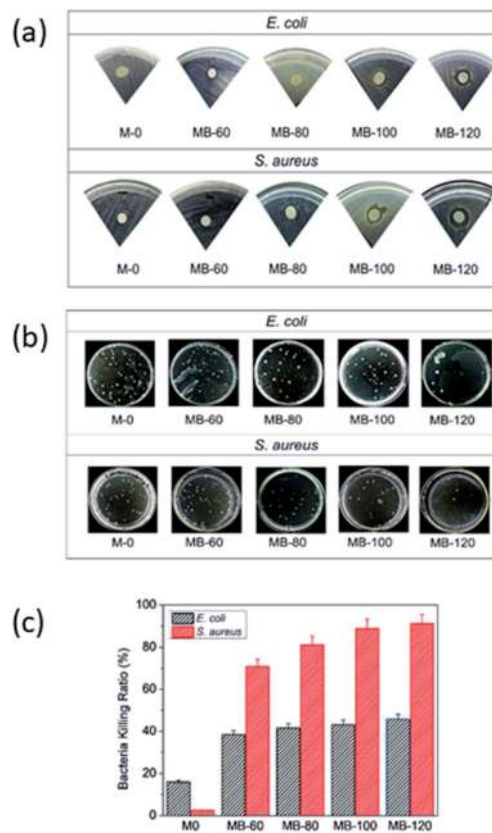

Fig. 1 (a) ZOI, (b) total plate count, and (c) bacteria-killing ratio of composite membranes, at different BKC contents against *E. coli* and *S. aureus*.

membranes, *i.e.*, chitosan and MWCNT.[43,44] The BKR increases in line with the BKC contents, up to 43.8 and 91.1% (MB-120) for *E. coli* and *S. aureus*, respectively.

The results indicate that the increase of BKC concentration in the composite membrane improve its antibacterial activity, where it is more effective for killing *S. aureus* than *E. coli*. This is likely due to differences in the BKC bacteriocidal mechanisms towards the outer structure of the cell membranes. In general, BKC induces cell death through several steps: (i) permeation of antibacterial agents into cell membranes, (ii) disruption of the cell membrane structures, which then induces (iii) leakages of the intracellular materials, followed by (iv) degradation or denature of proteins and nucleic acids, and (v) finally the cell damaged. Moreover, Gram-positive bacteria have peptidoglycan layers that are rich in teichoic acid. This promotes the N$^+$ moiety of BKC adsorption into the cell, lowering the resistance. In contrast, Gram-negative bacteria, such as *E. coli*, have special outer membrane layers that are resilient to antibacterial agents.[33,45,46] The results indicate that the increase of BKC loading improve the antibacterial activity of the membrane. It is slowly released, inhibiting and inactivating bacteria *via* various mechanisms.[30–32]

3.2. Physical appearance of composite membranes

Apart from the use of BKC antimicrobial agents, introduction of MWCNTs in to composite membranes were carried out to

enhance the membrane's mechanical properties.[47] The appearances of the composite membranes containing different contents of BKC are shown in the ESI (Fig. S1†). For M-0, a broken white dried membrane with wrinkled features was obtained. Membranes with similar appearance were obtained after adding BKC. After soaking in water, the resulting wet membranes exhibit a suitable shape with a smooth surface and homogeneous white colour. The surface of the M-0 membrane is glossy, while MB-120 shows a slightly matted surface.

3.3. Morphological and topological studies

FE-SEM and AFM microscopies were employed to evaluate the surface topographies of the composite membranes. A notable modification in the morphology was observed. M-0 exhibited a smooth and flat like surface. However, a porous structure with rougher surfaces was predominant in BKC-loaded membranes (Fig. 2). Among the samples prepared, MB-80 had the highest porosity (68%) and the largest average pore size (27 nm). These are valuable for the separation of bulk molecules (*e.g.* dyes). Nevertheless, a further increase in the BKC content (MB-100) led to a reduction in the porosity (64%) and average pore radius (23 nm), as depicted in Fig. S2.† This might be due to the occupation and blockage of hydrophobic moieties of BKC in the membrane pores. It was also observed that the average roughness (R_a) and the root mean square roughness (R_q) values increased with the addition of BKC. The R_a and R_q values increase from 0.063 and 0.074 μm to 0.167 and 0.187 μm, as summarized in Fig. S3.† This is likely caused by an aggregation of hydrophobic alkyl groups on the membrane surface. Segregation of BKC, as quaternary ammonium amphiphilic compound during the casting process, may be a major cause of this hydrophobic accumulation on the membrane surfaces.[48–50]

As PEG is utilized as a porogen in the fabrication of the porous membranes, its ability to form dispersed domains in the chitosan network and shift to the membrane surface is examined. The corresponding membranes after a year of storage were sonicated in DI water for at least 3 h. SEM images of their cross-sectional structures were then examined, as shown in Fig. 3. The shape of the pore structures is strongly dependent on the BKC contents, in which M-0 and MB-60 show well-dispersed spherical voids. In contrast, those with higher BKC contents, *i.e.*, MB-100 and MB-120, exhibit elongated pore structures. This is likely due to different structural formation mechanisms. In M-0 or at low BKC contents, PEG forms spherical domains (dispersed) in the matrix or acts as a surfactant, promoting compatibility between MWCNT and BKC with the hydrophilic chitosan. When the BKC content is increased, however, BKC tends to form a flattened structure from π–π stacking interactions with MWCNTs or among BKC/BKC molecules, as proposed in Fig. 3e. BKCs cationic species are located on the cluster surfaces, which are then stabilized by the hydrophilic PEG molecules. These elongated structures become more apparent when PEG is removed by migrating from the domains, as a result of a long storage time and the ultrasonication treatment. This is strongly supported by the results on mechanical, physical, and antimicrobial properties of the membranes, which are discussed later.

3.4. Hydrophilicity, mechanical properties, and thermal stability

As permeability of membranes is dependent on their hydrophilicity[40] and surface wettability, the WCA of the composite membranes was determined, as shown in Fig. 4. An increase in WCA values was observed after adding BKC, and further increased with the BKC contents (M-0 = 57.8°; MB-120 = 81.3°).
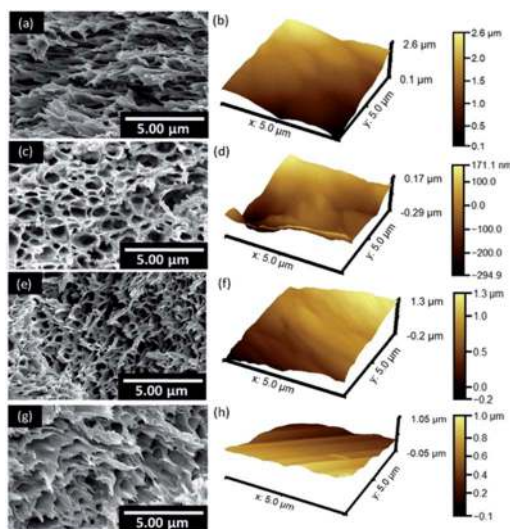

Fig. 2 SEM and AFM surface images of composite membranes containing different BKC contents: (a) and (b) M-0, (c) and (d) MB-60, (e) and (f) MB-80, and (g) and (h) MB-100.
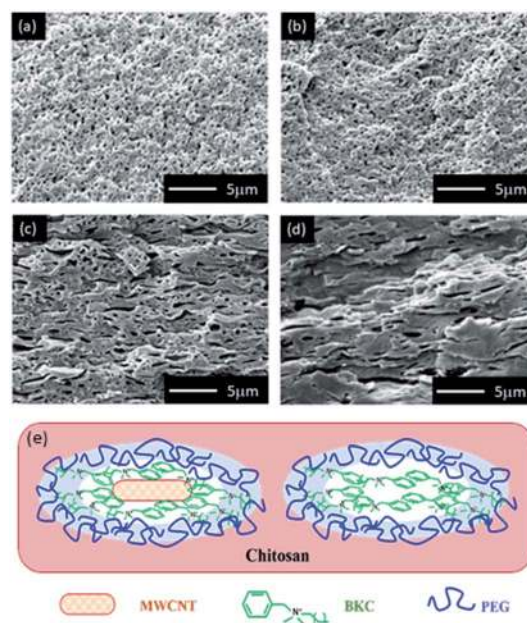

Fig. 3 SEM images of composite membranes after 1 year of storage and being incubated under sonication for 3 h: (a) M-0, (b) MB-60, (c) MB-100, (d) MB-120, and (e) proposed structures of the composite membranes.

This decrease in surface hydrophilicity likely originates from the hydrophobic alkyl moiety of BKC. Although BKC prefers to form clusters surrounded by PEG chains, as discussed earlier, an increase in its content relative to PEG leads to its accumulation on the membrane surfaces. This is also likely caused by the segregation of BKC, as amphiphilic quaternary ammonium compounds in the making of the casting solution (contact with air).[48] Additionally, an increment in the membrane surface roughness is perhaps caused by the decrease in surface hydrophilicity. This is in good agreement with the porosity % results. Nevertheless, since the WCA values of all composite membranes after adding BKC are still lower than 90°, these are categorized as hydrophilic membranes (<90°).[51]

To obtain insights into the PEG migration mechanism from the chitosan matrix, the surface wettability of the composite membranes after a year of storage (subject to sonicating treatment) was examined. The WCA values cannot be determined, as the water droplets were rapidly absorbed into the membrane, reflecting their hydrophilicity and/or highly porous surfaces. This confirms the migration of the PEG porogen to the membrane surfaces, which are then conveniently removed by the ultrasonication treatment.

The mechanical properties of the composite membranes were investigated by tensile experiments. The stress–strain curves are compared in Fig. 5. Interestingly, the mechanical properties of the membranes are strongly dependent on the BKC compositions. The tensile strength and Young's modulus slightly decreased with an increase in the BKC contents, due to the presence of the softer domains (consisting of PEG chains) dispersed in the stiffer chitosan matrix. However, drastic enhancements in the membrane's toughness were observed, reflected by large improvements in the elongation at break values as a function of the BKC contents, from 4% (M-0) to 42% (MB-120). This strongly supports the toughening effects from the formation of elongated dispersed domains of MWCNT/BKC/PEG clusters in the brittle chitosan matrix, as discussed earlier, which is in good agreement with others studies.[52,53] This enhancement in the toughness of the membranes as a function of BKC content, in addition to their intended antimicrobial/
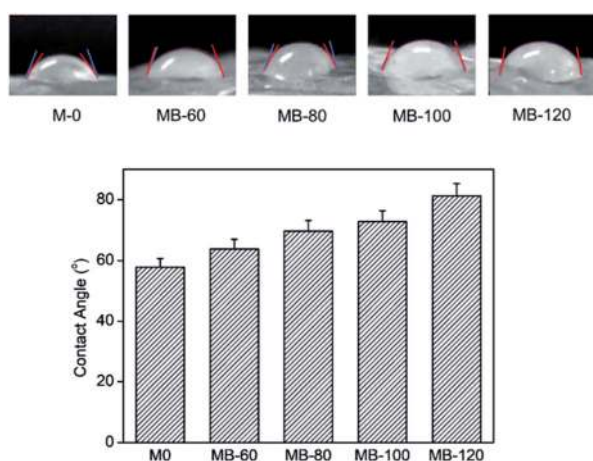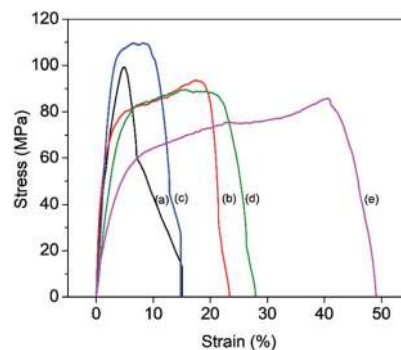

Fig. 5 Tensile stress–strain plots of composite membranes containing different BKC contents: (a) M-0, (b) MB-60, (c) MB-80, (d) MB-100, and (e) MB-120.

antifouling properties, provides additional advantages for practical use. The enhanced durability for ultrafiltration applications is especially useful.

The thermal resistance of the composite membranes was evaluated using thermal gravimetric analysis (TGA), as shown in Fig. S4.† The first weight-loss stage from room temperature to 450 K is due to the evaporation of moisture trapped inside the membranes with a content of approximately 11–19%. A major decomposition step (up to 40%) was observed from 450 to 630 K, corresponding to low molecular weight polymeric components. Finally, the weight-loss stage at temperatures higher than 630 K occurred due to acetylation and deacetylation of chitosan monomer.[54] The higher the BKC loading contents, the larger the weight loss of the composite membrane, since BKC has lower thermal stability (T_{max} = 481 K) than chitosan (T_{max} = 568 K). Thus, the addition of BKC into the composite membranes leads to a reduction in their thermal stability. The weakening of hydrogen bonding due to electrostatic repulsion of cationic groups from BKC also induces a decrease in the composite membrane crystallinity,[54] leading to a decrease in the composition of the final residues (Table S1†). Nevertheless, the decline of thermal stability is relatively low and indicates that the composite membranes have been successfully modified with BKC.

3.5. Physicochemical characterizations

The crystal structures of the membranes were analysed by X-ray diffraction (XRD) spectroscopy, as shown in Fig. 6. Neat chitosan exhibited broad signals at 2θ = 20.1 and 10.1°, corresponding to its (020) and (200) lattice structures, respectively. The presence of these signals and their broad shoulder peaks reveals that it is semi-crystalline.[3] All composite membranes exhibited sharper signals at 19.9 and 22.1°, which overlap with that of the chitosan signal. These diffraction peaks originate from the PEG structure.[55,56] The signal of MWCNT was expected at 18°, corresponding to the interlayer spacing of the nanotube (002) and the (100) reflection of the carbon atoms.[57] However, these cannot be detected due to the relatively low content of MWCNT in the composites. The sharp signals of PEG and the narrower signals of chitosan at 10.1 and 20.1° in all membranes

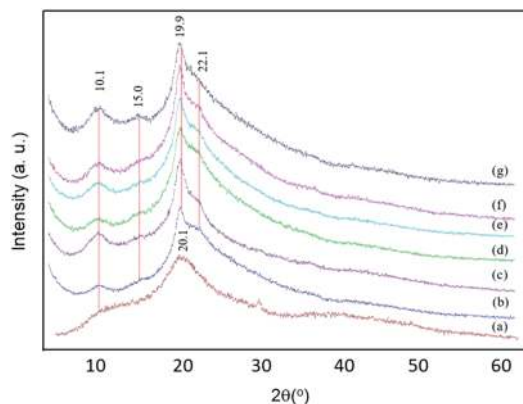
Fig. 4 Water contact angle of the composite membranes.

Fig. 6 XRD traces: (a) neat chitosan, and composite membranes with different BKC contents: (b) M-0, (c) MB-60, (d) MB-80, (e) MB-100, (f) MB-120, and (g) MB-400.
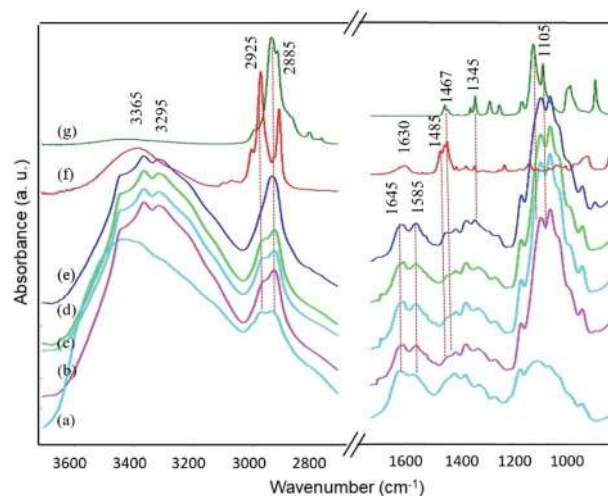

Fig. 7 FTIR spectra of freshly prepared composite membranes with various BKC contents: (a) neat chitosan, (b) M-0, (c) MB-60, (d) MB-80, (e) MB-120, (f) BKC, and (g) PEG.

indicate a phase reorganization of the polymeric components. The hydrophilic moieties of chitosan (*e.g.* –OH group) interact with PEG, leading to crystalline phase formation. Interestingly, a new signal was observed at 15.0°. This signal intensity increased with an increase in the BKC contents. This signal corresponds to a *d*-spacing of 0.59. This likely originates from BKC clusters, generated by the π–π stacking of BKC's aromatic rings or the BKC ring with those of MWCNT, which are covered by PEG, as discussed earlier. This further enhances the compatibility of BKC with the chitosan network, leading to uniform dispersions of the nanoclusters in the composite membranes.

The proposed chemical structures and interactions among BKC and the membrane components were further investigated using FTIR spectroscopy. Fig. 7 demonstrates ATR-FTIR spectra of freshly-prepared composite membranes with various BKC contents. The characteristic bands of chitosan were observed at 3365, 3295, 1645, and 1585 cm^{-1}, corresponding to the O–H/N–H stretching modes, the C=O stretching of amide I, and the N–H bending mode. All composite membranes show the typical bands of PEG at 2885, 1467, 1345, and 1105 cm^{-1}, and those of BKC at 2925, 1630, and 1485 cm^{-1}. The results confirm that BKC and PEG, likely in the form of PEG-coated nanoclusters, are homogeneously dispersed in the chitosan matrix by predominantly forming hydrogen bonds.[58] The bands of MWCNT cannot be observed in the spectra due to the low IR-active nature of its functional groups and its small concentration in the matrix. An increase in the intensity of the strong bands in the 1105 cm^{-1} region, associated with the C–O–C stretching mode, of the composite membranes compared to that of neat chitosan reflects a presence of PEG, especially on the surface of the membranes. To examine the relative content of BKC, its characteristic bands at 2925 and 1485 cm^{-1} are employed. In contrast, the bands at 2885 and 1467 cm^{-1} are unique for PEG. The intensity ratio of the 2925/2885 cm^{-1} band increases with the BKC content in the composite membranes, except in MB-120, where anomalous PEG characteristic dominates. However, the increase in the relative BKC/PEG contents is clearly reflected by the corresponding ratio of the 1485/

1467 cm^{-1} band. This indicates the dispersion of BKC and PEG, especially at the membrane surfaces. This notably agrees with other results.[59]

The stability of PEG porogen in the membrane structure was examined. ATR-FTIR spectra of the membranes were re-examined after one year of storage time, as shown in Fig. 8. All spectra are different from those of the freshly-prepared membranes, in which vibrational modes due to PEG are dominant features. The ATR-FTIR spectra mainly exhibit vibrational modes of functional moieties located on the membrane surface. Hence, most PEG chains move to the membrane surface as a function of time, likely because of their incompatibility with chitosan and its high mobility due to the short-chain structure.
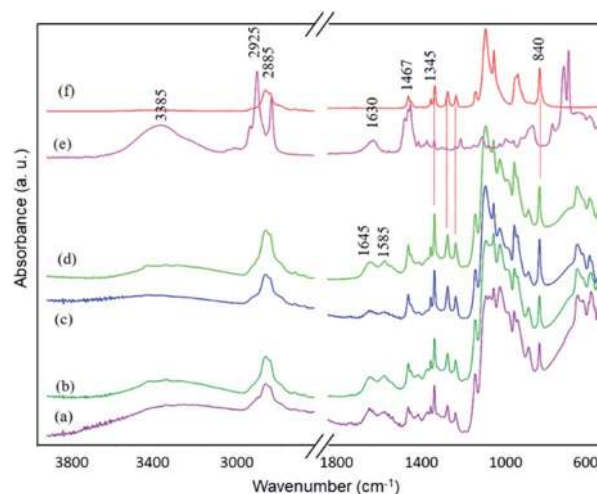

Fig. 8 FTIR spectra of composite membranes with various BKC contents after 1 year of storage: (a) M-0, (b) MB-60, (c) MB-80, (d) MB-120, (e) BKC, and (f) PEG.

When the membranes were treated by sonication in water, however, PEG molecules were completely removed from the surface. This is reflected by their ATR-FTIR spectra, as shown in Fig. 9, in which the vibrational modes of PEG disappeared, and the characteristic bands of chitosan and BKC were recovered. The relative intensity of the band at 2925 cm^{-1}, a characteristic of BKC, was higher than that of the corresponding freshly-prepared membranes with the same BKC content (Fig. 7). This indicates that BKC also migrates to the surface along with PEG, confirming the existent of its nanocluster structures, covered by PEG chains.

3.6. Permeation test

The performance of the resulting composites as filter membranes was examined by a dead-end filtration system. The results are summarized in Fig. 10a. The deionized water flux through the membranes was significantly reduced upon the incorporation of BKC. This is probably due to membrane fouling induced by the perpendicular pressure exerted on the membrane surface. Accordingly, the retained particles are deposited on the membrane surface, forming a filtration-cake layer. This leads to a decrease in hydrophilicity and pore size of the composite membranes upon the BKC addition. Consequently, the water permeability decreases, caused by the increase of surface tension for water-molecule infiltration through the pores, hindering water molecules from passing through the membrane.[38] A further increase in the BKC contents leaded to decreased water flux, however. This is likely because of reduced surface hydrophilicity.

The results on dye and BSA rejection by dead-end filtration are summarized in Fig. 10b. The membrane rejection performances toward the azo blue dyes were increased as a function of the BKC loading (M-0: 22%; MB-60: 48%; and MB-100: 72%). An increase in the BKC composition induces a high positive charge on the membrane surface that facilitates the interfacial
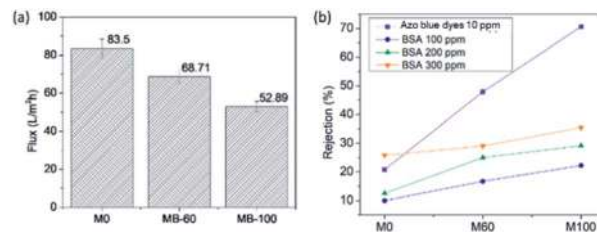

Fig. 10 The results on (a) average water flux during a 10 min filtration process, and (b) rejection % of the composite membranes using a dead-end filtration system toward dye and BSA.

attachment of the negatively-charged dye molecules *via* electrostatic attractions.[48] This leads to higher contents of dye molecules accumulated on the membrane surface. A similar tendency was found for BSA rejection where the membrane rejections were increased as a function of the BKC content, even though the rejection percentage was smaller than that of the azo dye molecules. This can be explained by two factors. First, electrostatic attraction between negatively-charged BSA molecules (isoelectric point 4.4, pH 7) and positive charges on the surface led to the aggregation of BSA on the membrane surface. Second, BSA has a larger molecular weight and molecular structure (M_w = 66 kDa) than the azo blue dyes (M_w = 7.74 kDa), thus impeding the interactions on the membrane surface. The higher the BSA content, the larger the rejection by the composite membranes. Regarding the results, the membranes have high potential in wastewater treatment for reducing bacterial fouling, without decreasing the water separation performance.

To assess long-term performances and stability of the membranes, their antibacterial properties after a year of storage and an extensive sonication in water were examined (Fig. S5†). The bacterial killing ratios slightly decrease at around 3–5%, compared to those of the freshly-prepared counterparts (Fig. S6†). In addition, the results on average water flux of the membranes for up to 3 cycles of operation were examined (Fig. S7†). The membranes with no BKC and low BKC content, M0 and M-60, show slight drops in the performance. The corresponding values for the membrane with a high content of BKC, M-100, however are almost unchanged. According to the National Institute for Occupational Safety and Health, the lowest oral toxic dose of BKC for a human is 266 mg kg^{-1}. The concentration of BKC in the composite membranes used in this study is lower than the toxic dosage. Although the results suggest that BKC is immobilized in the membrane matrix with high stability, the concentration of BKC, which may be leach out from the membranes and soluble in the water, was measured by UV-Vis spectroscopy. The results show that 0.42 ppm (M-50) and 0.57 ppm (M-100) of released BKC was detected. This confirms that the application of these membranes has no risks for human as well as the environment.

4. Conclusions

Chitosan-based composite membranes with antibacterial properties and enhanced toughness have been successfully
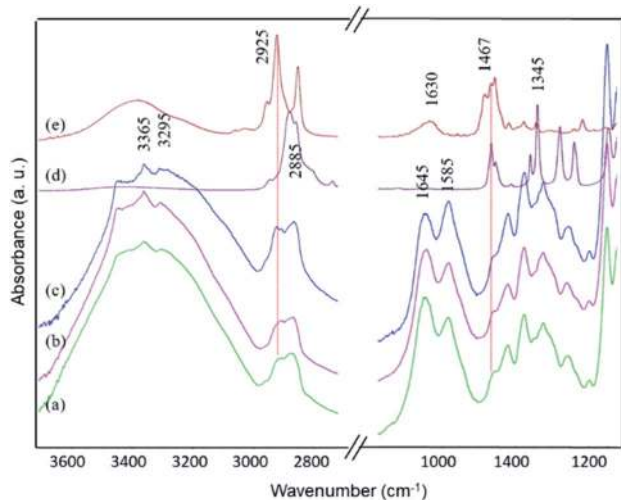

Fig. 9 FTIR spectra of composite membranes with various BKC contents, which were stored for 1 year, after being sonicated in water for 3 h: (a) M-0, (b) MB-60, (c) MB-120, (d) PEG, and (e) BKC.

prepared by employing BKC. The results from SEM, XRD, and FTIR spectroscopy reveal that MWCNT/BKC is located as nanoclusters by π–π stacking interactions, which are coved by PEG chains. This leads to the formation of dispersed domains in the chitosan matrix. The shape of the dispersed domains is spherical at low BKC contents, but becomes elongated shape with an increase in the BKC contents. These act as soft domains with an anisotropic shape, to toughen the brittle chitosan matrix. Furthermore, the BKC incorporation into the composite membranes increases the antibacterial efficacy against *S. aureus* and *E. coli* due to the antibacterial properties of BKC. The BKC addition also modifies the surface and improves the toughness of the membranes. This results in enhancements of membrane rejection and stability. The composite membrane is beneficial from environmental and economic perspectives. They are easy to prepare, low-cost, and not detrimental to the environment. The materials are promising for practical use in highly-efficient dye removal, inhibiting biofilm formation and biofouling.

Author contributions

Fitri Khoerunnisa: conceptualization, methodology, writing – original draft, funding acquisition. Chintia Kulsum: investigation, analysis. Fitri Dara: investigation, analysis. Mita Nurhayati: writing – original draft, visualization. Nisa Nashrah: investigation, analysis. Siti Fatimah: investigation, analysis. Amelinda Pratiwi: writing – original draft. visualization. Hendrawan: writing – review & editing. Muhamad Nasir: resources, writing – review & editing. Young Gun Ko: resources. Eng-Poh Ng: resources. Pakorn Opaprakasit: conceptualization, methodology, writing – review & editing, supervision.

Conflicts of interest

There are no conflicts to declare.

Acknowledgements

References

1 N. Ali, A. Khan, S. Malik, S. Badshah, M. Bilal and H. M. Iqbal, *J. Environ. Chem. Eng.*, 2020, **8**, 104064.
2 M. Kamrani, A. Akbari and A. Y. Lehi, *J. Environ. Chem. Eng.*, 2018, **6**, 583–587.
3 M. Sai, R. Guo, L. Chen, N. Xu, Y. Tang and D. Ding, *J. Appl. Polym. Sci.*, 2015, **132**, 1–9.
4 Y. Feng, X. Lin, H. Li, L. He, T. Sridhar, A. K. Suresh, J. Bellare and H. Wang, *Ind. Eng. Chem. Res.*, 2014, **53**, 14974–14981.
5 R. Weng, X. Huang, D. Liao, S. Xu, L. Peng and X. Liu, *RSC Adv.*, 2020, **10**(3), 1309–1318.
6 S. Ayyaru and Y. H. Ahn, *J. Membr. Sci.*, 2017, **525**, 210–219.
7 S. R. Mousavi, M. Asghari and N. M. Mahmoodi, *Carbohydr. Polym.*, 2020, **237**, 11628.
8 J. Shao, B. Wang, J. Li, J. A. Jansen, F. Walboimers and F. Yang, *Mater. Sci. Eng., C*, 2019, **98**, 1053–1063.
9 E. Bagheripour, A. R. Moghadassi, S. M. Hosseini, B. VanderBruggen and F. Parvizian, *J. Ind. Eng. Chem.*, 2018, **62**, 311–320.
10 A. Behboudi, Y. Jafarzadeh and R. Yegani, *J. Environ. Chem. Eng.*, 2018, **6**, 1764–1773.
11 K. L. Ly, C. B. Raub and X. Luo, *Mater. Adv.*, 2020, **1**(1), 34–44.
12 X. Zhao, R. Zhang, Y. Liu, M. He, Y. Su, C. Gao and Z. Jiang, *J. Membr. Sci.*, 2018, **551**, 145–171.
13 H. Nagahama, H. Maeda, T. Kashiki, R. Jayakumar, T. Furuike and H. Tamura, *Carbohydr. Polym.*, 2009, **76**, 225–260.
14 L. Shen, X. Pei, J. Han, T. Zhang, P. Li and X. Wang, *Colloids Surf., A*, 2019, **569**, 145–155.
15 K. V. Otvagina, A. V. Penkova, M. E. Dmitrenko, A. I. Kuzminova, T. S. Sazanova, A. V. Vorotyntsev and I. V. Vorotyntsev, *Membranes*, 2019, **9**(3), 38.
16 B. Zhang, J. Fu, Q. Zhang, C. Yi and B. Yang, *J. Appl. Polym. Sci.*, 2019, **136**, 47848.
17 U. Habiba, A. M. Afifi, A. Salleh and B. C. Ang, *J. Hazard. Mater.*, 2017, **322**, 182–194.
18 J. Kim and B. Van der Bruggen, *Environ. Pollut.*, 2010, **158**, 2335–2349.
19 J. Zhu, J. Hou, Y. Zhang, M. Tian, T. He and J. Liu, *J. Membr. Sci.*, 2018, **550**, 173–197.
20 Y. Qi, L. Zhu, C. Gao and J. Shen, *RSC Adv.*, 2019, **9**(11), 6107–6117.
21 F. A. A. Ali, J. Alam, A. K. Shukla, M. Alhooshan, M. A. Ansari, W. A. Al-Masry, S. Rehman and M. Alam, *React. Funct. Polym.*, 2019, **140**, 136–147.
22 I. Munawar, S. S. Iqbal, M. N. Anwar, M. Batool, S. Tariq, N. Faitma, A. L. Khan, A. U. Khan, U. Nazar, T. Jamil and M. N. Ahmad, *Carbohydr. Polym.*, 2017, **175**, 661–670.
23 Y. Du, Y. Li and T. Wu, *RSC Adv.*, 2017, **7**(66), 41838–41846.
24 F. Khoerunnisa, W. Rahmah, B. S. Ooi, E. Dwihermiati, N. Nashrah, S. Fatimah, Y. G. Ko and E. P. Ng, *J. Environ. Chem. Eng.*, 2020, **8**, 1030686.
25 W. Wang, L. Zhu, B. Shan, C. Xie, C. Liu, F. Cui and G. Li, *J. Membr. Sci.*, 2018, **548**, 459–469.
26 A. Cihanoglu and A. Altinkaya, *J. Membr. Sci.*, 2020, **594**, 117438.
27 M. Chen, X. Zhang, Z. Wang, L. Wang and Z. Wu, *Water Res.*, 2017, **120**, 256–264.
28 M. Ping, X. Zhang, M. Liu, Z. Wu and Z. Wang, *J. Membr. Sci.*, 2019, **570**, 286–293.
29 Y. Zhai, X. Zhang, Z. Wu and Z. Wang, *J. Membr. Sci.*, 2020, **597**, 117679.
30 X. Zhang, Z. Wang, M. Chen, J. Ma, S. Chen and Z. Wu, *J. Membr. Sci.*, 2017, **539**, 229–237.

31 U. Tezel and S. G. Pavlostathis, *Curr. Opin. Biotechnol.*, 2015, **33**, 296–304.

32 G. Kampf, *Journal of Hospital Infection*, 2018, **100**, e1–e22.

33 S. Bondurant, T. McKinney, L. Bondurant and L. Fitzpatrick, *Am. J. Infect. Control*, 2020, **48**(5), 522–526.

34 J. Tessier and A. R. Schmitzer, *RSC Adv.*, 2020, **10**(16), 9420–9430.

35 A. Fazlara and M. Ekhtelat, *Am.–Eurasian J. Agric. Environ. Sci.*, 2012, **12**, 23–29.

36 P. C. Rath, B. P. Singh, L. Besra and S. Bhattacharjee, *J. Am. Ceram. Soc.*, 2012, **95**(9), 2725–2731.

37 A. Kroustalli, A. E. Zisimopoulou, S. Koch, L. Rongen, D. Deligianni, S. Diamantouros, G. Athanassiou, M. Kokozidou, D. Mavrilas and S. Jockenhoevel, *J. Mater. Sci.: Mater. Med.*, 2013, **24**(12), 2889–2896.

38 M. S. A. Saraswathi, S. Mahalakshmi, S. Vetrivel, K. Divya, D. Rana and A. Nagendran, *J. Environ. Chem. Eng.*, 2018, **6**(2), 1912–1917.

39 H. Yajima, M. Morita, M. Hashimoto, H. Sashiwa, T. Kikuchi and T. Ishii, *Int. J. Thermophys.*, 2001, **22**(4), 1265–1283.

40 H. B. Li, W. Y. Shi, Y. F. Zhang, D. Q. Liu and X. F. Liu, *Polymers*, 2014, **6**, 1846–1861.

41 M. Aktera, M. T. Sikderbcd, M. M. Rahmana, A. K. M. A. Ullah, K. F. B. Hossain, S. Banik, T. Hosokawa, T. Saito and M. Kurasaki, *J. Adv. Res.*, 2018, **9**, 1–16.

42 Y. Liu, H. Huang, P. Huo and J. Gu, *Carbohydr. Polym.*, 2017, **165**, 266–275.

43 M. Liu, G. Luo, Y. Wang, R. Xu, Y. Wang, W. He, J. Tan, M. Xing and J. Wu, *Sci. Rep.*, 2017, **7**, 436.

44 M. Kaya, S. Khadem, Y. S. Cakmak, M. Mujtaba, S. Ilk, L. Akyuz, A. M. Salaberria, J. Labidi, A. H. Abdulqadir and E. Deligöz, *RSC Adv.*, 2018, **8**(8), 3941–3950.

45 S. Zhang, J. Li, J. Li, N. Du, D. Li, F. Li and J. Man, *RSC Adv.*, 2020, **10**(56), 34308–34322.

46 J. Pant, J. Gao, M. J. Goudie, S. P. Hopkins, J. Locklin and H. Handa, *Acta Biomater.*, 2017, **58**, 421–431.

47 M. Adeel, L. F. Ren, J. Li, J. Shao, A. Jawad, C. Su, Y. Wang, L. Guo and Y. He, *J. Appl. Polym. Sci.*, 2019, **136**, 47123.

48 M. B. Harney, R. R. Pant, P. A. Fulmer and J. H. Wynne, *ACS Appl. Mater. Interfaces*, 2009, **1**(1), 39–41.

49 J. Meng, X. Zhang, L. Ni, Z. Tang, Y. Zhang, Y. Zhang and W. Zhang, *Desalination*, 2015, **359**, 156–166.

50 S. Wang, Y. Liu, S. Huang, H. Wu, Y. Li, Z. Tian and Z. Jiang, *J. Membr. Sci.*, 2014, **460**, 62–70.

51 L. Zou, P. Gusnawan, G. Zhang and J. Yu, *J. Membr. Sci.*, 2020, **615**, 118552.

52 K. Katsumata, T. Saito, F. Yu, N. Nakamura and Y. Inoue, *Polym. J.*, 2011, **43**(5), 484–492.

53 L. M. Nanjegowda, R. Bommulu, V. Juikar and S. Hatna, *Ind. Eng. Chem. Res.*, 2013, **52**(16), 5672–5682.

54 S. Sun, Q. An, X. Li, L. Qian, B. He and H. Xiao, *Bioresour. Technol.*, 2010, **101**(14), 5693–5700.

55 J. Venkatesan, Z. J. Qian, B. Ryu, N. A. Kumar and S. K. Kim, *Carbohydr. Polym.*, 2011, **83**(2), 569–577.

56 X. Fu, Y. Xiao, K. Hu, J. Wang, J. Lei and C. Zhou, *Chem. Eng. J.*, 2016, **291**, 138–148.

57 C. Gau, H. S. Ko and H. T. Chen, *Nanotechnology*, 2009, **20**, 185503.

58 N. Zhou, N. Meng, Y. Ma, X. Liao, J. Zhang, L. Li and J. Shen, *Carbon*, 2009, **47**(5), 1343–1350.

59 V. Nayak, M. S. Jyothi, R. G. Balakrishna, M. Padaki and A. F. Ismail, *ChemistryOpen*, 2015, **4**, 278–287.